

Article

Hydrogen Yield from CO₂ Reforming of Methane: Impact of La₂O₃ Doping on Supported Ni Catalysts

Ahmed Abasaheed ¹, Samsudeen Kasim ¹, Wasim Khan ^{1,2,*}, Mahmud Sofiu ¹, Ahmed Ibrahim ¹,
Anis Fakeeha ^{1,3} and Ahmed Al-Fatesh ¹

¹ Chemical Engineering Department, College of Engineering, King Saud University, P.O. Box 800, Riyadh 11421, Saudi Arabia; abasaheed@ksu.edu.sa (A.A.); sofkolajide2@gmail.com (S.K.); mahmudsofiu@gmail.com (M.S.); aididwthts2011@gmail.com (A.I.); anishf@ksu.edu.sa (A.F.); aalfatesh@ksu.edu.sa (A.A.-F.)

² Department of Chemical and Process Engineering, University of Canterbury, 20 Kirkwood Avenue, Upper Riccarton, Christchurch 8041, New Zealand

³ King Abdullah City for Atomic & Renewable Energy, Energy Research & Innovation Center (ERIC) in Riyadh, Riyadh 11451, Saudi Arabia

* Correspondence: wasimkhan49@gmail.com

Abstract: Development of a transition metal based catalyst aiming at concomitant high activity and stability attributed to distinguished catalytic characteristics is considered as the bottleneck for dry reforming of methane (DRM). This work highlights the role of modifying zirconia (ZrO₂) and alumina (Al₂O₃) supported nickel based catalysts using lanthanum oxide (La₂O₃) varying from 0 to 20 wt% during dry reforming of methane. The mesoporous catalysts with improved BET surface areas, improved dispersion, relatively lower reduction temperatures and enhanced surface basicity are identified after La₂O₃ doping. These factors have influenced the catalytic activity and higher hydrogen yields are found for La₂O₃ modified catalysts as compared to base catalysts (5 wt% Ni-ZrO₂ and 5 wt% Ni-Al₂O₃). Post-reaction characterizations such as TGA have showed less coke formation over La₂O₃ modified samples. Raman spectra indicates decreased graphitization for La₂O₃ catalysts. The 5Ni-10La₂O₃-ZrO₂ catalyst produced 80% hydrogen yields, 25% more than that of 5Ni-ZrO₂. 5Ni-15La₂O₃-Al₂O₃ gave 84% hydrogen yields, 8% higher than that of 5Ni-Al₂O₃. Higher CO₂ activity improved the surface carbon oxidation rate. From the study, the extent of La₂O₃ loading is dependent on the type of oxide support.

Keywords: Al₂O₃; CO₂ reforming; La₂O₃; CH₄; ZrO₂



Citation: Abasaheed, A.; Kasim, S.; Khan, W.; Sofiu, M.; Ibrahim, A.; Fakeeha, A.; Al-Fatesh, A. Hydrogen Yield from CO₂ Reforming of Methane: Impact of La₂O₃ Doping on Supported Ni Catalysts. *Energies* **2021**, *14*, 2412. <https://doi.org/10.3390/en14092412>

Academic Editors: Vladislav A. Sadykov and Wasim Khan

Received: 2 March 2021

Accepted: 20 April 2021

Published: 23 April 2021

Publisher's Note: MDPI stays neutral with regard to jurisdictional claims in published maps and institutional affiliations.



Copyright: © 2021 by the authors. Licensee MDPI, Basel, Switzerland. This article is an open access article distributed under the terms and conditions of the Creative Commons Attribution (CC BY) license (<https://creativecommons.org/licenses/by/4.0/>).

1. Introduction

The decrease of fossil fuel energy and the dilemma of environmental pollution urged a large number of researchers to maximize the conversions of methane and carbon dioxide into useful products such as hydrogen. Hydrogen is a benign source of energy. It is mainly obtained from biomass pyrolysis and thermal reforming. Methane, the main component of natural gas, can be obtained from various resources like shale gas and the fracking process, which has increased the availability of natural gas from infrequent deposits [1,2]. Moreover, the utilization of biogas is gaining momentum in recent years [3,4]. In the field of heterogeneous catalysis, particularly, in the latest decades, dry reforming of methane is regarded as one of the best prospective ways of conversion [5–7]. However, the dry reforming reaction as shown in Equation (1) is highly endothermic and thus requires high reaction temperatures. The process produces synthesis gas that has an appropriate ratio of H₂ to CO suitable for Fischer–Tropsch synthesis [8]. Steam reforming of methane remains the best available industrial process for generating synthesis gas [9,10]. The requirement and the utilization of synthesis gas production are continuously increasing [11]. During methane dry reforming (DRM), CO₂ is employed as an oxidant, which draws the interest

and the likelihood of seizing and recycling CO₂ from the exhaust flue gases of industrial and power plants. DRM is presently not industrially applied because of the heavy coking and sintering of the catalysts in high-temperature reforming reactions [12]. Thus, it is essential to find an innovative catalyst that endures sintering and coking. The sintering of the metallic phase and carbon formation on the surface of the catalyst, which causes the deactivation, originate from operating conditions that facilitate the side reactions, which involve the cracking of the CH₄ Equation (2) and the reverse Boudouard reaction Equation (3) resulting from the combinations of CO [13].



H₂ yield through DRM is significantly affected by dissociation of CH₄ over Ni-supported surface and the gasification of carbon formed by CO₂. The reverse water gas shift reaction and the action of the H₂ spillover on the surface affect the H₂ yield substantially. The hydrogen spill over enhances hydroxyl formation and catalytic activity toward CO oxidation at the metal/oxide interface. The hydroxyl groups at the metal/support interface react with CO to produce CO₂. Similarly, the reverse water gas shift (CO₂ + H₂O → CO + H₂) reduces the hydrogen; hence, the two phenomena involve the depletion of hydrogen and in turn influence the hydrogen yield. Noble metals like Pd, Ir, Pt, and Rh provide the extremely good performance of activity and stability but they are rare and expensive [14,15]. Transition metals like Ni are suitable alternatives for this reaction as they are stable and environmentally friendly [16,17]. Nonetheless, Ni-based catalysts are hampered by poor activity due to coke formations and sintering [18,19]. Hence, the major challenge is to come up with Ni catalysts capable of resisting carbon formation and sintering. Carbon generation may be opposed by controlling the reaction kinetics using suitable catalysts with proper constituents and supports. It has been established that metal–support interactions can alter both catalyst activity and activity maintenance. Bradford and Vannice had shown that support decoration of metal particle surfaces shattered big ensembles of metal atoms that served as active sites for carbon deposition and the sites in the metal–support interfacial region enhanced catalyst activity [20]. The choice of support type plays a vital role in DRM. Supports that possess O₂ species at the surface of the catalyst help the carbon oxidation on the metal [21,22]. The balance between the rate of methane decomposition and the rate of carbon gasification regulates the catalyst stability [23]. The preparation of mesoporous oxides, like Al₂O₃, possessing high surface area and precise pores have revealed motivating results to disperse the metal over the support structure [24–26]. Bian et al., in their investigation of Ni supported home-made mesoporous alumina in methane dry reforming, indicated that the formation of NiAl₂O₄ spinel is advantageous to activity and stability towards DRM reaction [27].

Newnham et al. synthesized nanostructured Ni-incorporated mesoporous alumina with various Ni loadings by hydrothermal method and tested them as catalysts for CO₂ reforming of methane [28]. The result displayed excellent stability when 10%Ni was used due to the fact that the Ni nanoparticles in these catalysts being highly stable towards migration/sintering under the reaction conditions. The presence of strong Ni–support interaction and/or active metal particles being confined to the mesoporous channels of the support. Al-Fatesh et al. studied dry reforming of methane using a series of nickel-based catalysts supported on γ-alumina promoted by B, Si, Ti, Zr, Mo, and W [5]. They concluded that the promoters enhanced the interaction between NiO and γ-alumina support and, hence, Ni dispersion and stability. On the other hand, ZrO₂ is prominent support with high thermal stability able to go through alteration in their acid–basic sites [29]. Numerous studies have displayed that the presence of ZrO₂ improves the thermal resistance, redox properties, oxygen storage capacity and gasification of deposited carbon [30,31]. Hu et al. examined the dry reforming of methane over Ni/ZrO₂ catalysts prepared via

decomposition of nickel precursor under the influence of dielectric barrier discharge (DBD) plasma at ~ 150 °C [32]. It was found to improve activities due to the exposition of Ni (111) facets, smaller metal particles, and more tetragonal zirconia with increased oxygen vacancies. In the course of dry reforming of methane, oxygen species over the catalyst surface affected the catalytic performance and carbon deposition. Zhang et al. studied the effects of the surface adsorbed oxygen species tuned by doping with metals like La, Ce, Sm, and Y on the catalytic behavior [33]. Their results confirmed that the surface adsorbed oxygen species promoted both CO₂ activation and CH₄ dissociation. Doping La₂O₃ in supported Ni catalysts favor the CO₂ adsorption on the surface of the catalyst [34], alters the chemical and electronic state of Ni at the interface with the support and decreases the chemical interaction between Ni and the support causing the intensification of reducibility and higher dispersion of nickel [35]. Tran et al. studied the enhancement of La₂O₃ in the physicochemical features of cobalt supported over alumina for DRM using different temperatures and feed compositions [36]. Their results displayed that the La₂O₃ improved the H₂ activation; enriched oxygen vacancy and lowered the apparent activation energy of CH₄ consumption. The work of Lui et al. elaborated the promotional effects of La, Al, and Mn on Fe-modified clay supported by Ni catalysts used for dry reforming of methane [37]. The result of adding La, Al, and Mn altered the surface area, the basicity of the catalysts, and produced a smaller metallic Ni size. Moreover, Yabe et al. performed dry reforming of methane using several transition metals supported on ZrO₂ catalysts [38]. Their results exhibited high activity and low carbon deposition upon using 1 wt%Ni/10 mol%La-ZrO₂ catalysts.

In the present work, we assess the effect of the lanthanum oxide as a textual promoter of alumina and zirconia supports over Ni catalysts in the catalytic reforming of CH₄ with CO₂. The impact of different loadings of lanthanum oxide will be examined and their influence on the hydrogen yield. The output data will be further associated with the characterization results of BET, XRD, TPR, TEM, TPD, and TGA before and after the reaction. The difference in the basic supports originating from alumina and zirconia in terms of sintering and coking will be explored.

2. Materials and Methods

2.1. Materials

Mesoporous γ -Al₂O₃ (purity 99.99%, purchased from Norton Co (New York, NY, USA)), precursor of zirconium oxide (ZrOCl₂·8H₂O, purity >99.0%, purchased from Fluka Chemika (Washington, DC, USA)), precursors of La₂O₃ and Ni, respectively, (La(NO₃)₃·6H₂O and Ni(NO₃)₂·6H₂O purchased from Sigma Aldrich (St. Louis, MO, USA)), double distilled water.

2.2. Catalyst Preparation

In the case of zirconium-based support (for 5Ni-10La-ZrO₂), the required amounts of zirconia (2.62 g) in the form of ZrOCl₂·8H₂O was ground completely and poured into the empty crucible. Then, the desired weights of La(NO₃)₃·6H₂O (0.265 g) and that of Ni(NO₃)₂·6H₂O (0.25 g) were added to the crucible containing the support to get a powder mixture. The mixture was ground well in the crucible to obtain a homogenous mixture. Purified water was poured slowly to the mixture to produce a paste while mixing. The paste was set to evaporate under room temperature condition until it dried. Thereafter, the dried sample was calcined at 700 °C for 3 h. The obtained catalysts were denoted as 5Ni-ZrO₂ for 5 wt% Ni supported over ZrO₂, and 5Ni-xLa-ZrO₂, where x = 10, 15, 20 wt%.

In the case of alumina-based support, the above-mentioned procedure was adopted by replacing zirconia with the required amounts of mesoporous γ -Al₂O₃. The obtained catalysts were denoted as 5Ni-Al₂O₃ for 5 wt% Ni supported over Al₂O₃ and 5Ni-xLa-Al₂O₃, where x = 10, 15, 20 wt%.

2.3. Catalyst Characterization and Activity

The catalyst activity test and characterization are described in detail in the supplementary information.

3. Results and Discussion

The surface texture of the catalysts was assessed via the nitrogen adsorption–desorption isotherms. Figure 1A shows the nitrogen adsorption isotherms of the fresh catalysts (5Ni-xLa₂O₃-ZrO₂, x = 0, 10, 15, and 20 wt%) and according to IUPAC labelling, catalysts are showing type IV isotherm with capillary condensation appearing at a relative pressure below the saturation pressure, and H1 hysteresis loop. These features are associated with mesoporous materials that have cylindrical pore geometry with narrow size distribution as well as relatively high uniformity [39]. Figure 1B exhibits the nitrogen adsorption isotherms of the fresh catalysts (5Ni-x%La-Al₂O₃). All samples indicate typical type IV adsorption/desorption isotherms with H1 hysteresis loop. Point of inflection at a relative pressure in the range of 0.6–0.75 corresponds to the capillary condensation which indicates the uniformity of the pores in mesoporous material [40,41]. The textural properties of the catalyst are given in Table S1 of the supplementary.

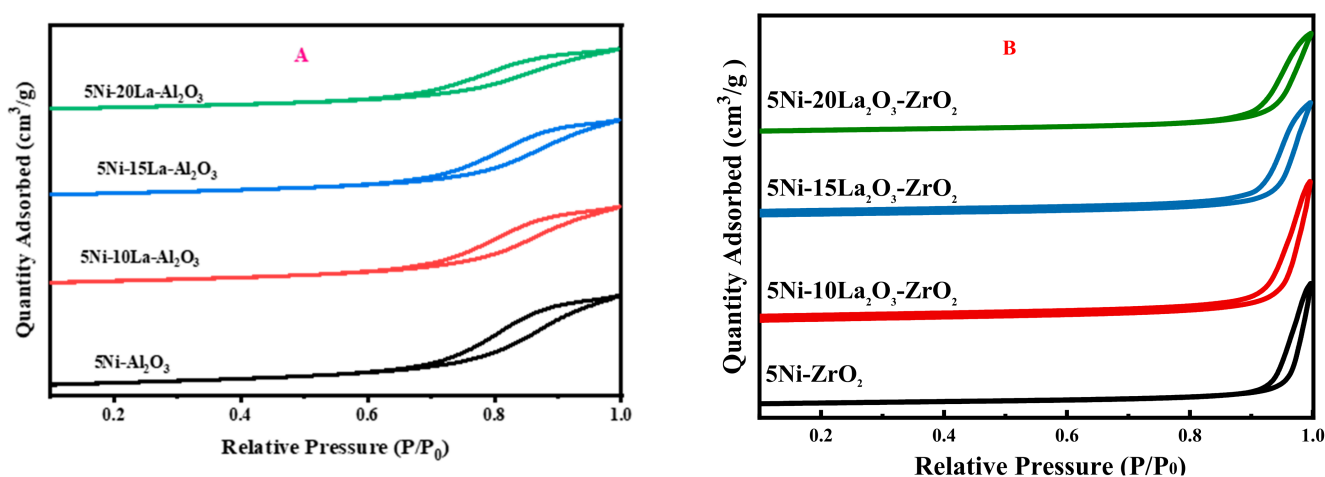


Figure 1. N₂ adsorption–desorption isotherms for fresh (A) 5Ni-xLa₂O₃+ZrO₂ and (B) 5Ni-x La₂O₃+Al₂O₃ catalyst calcined at 700 °C, (x = 0, 10, 15, and 20 wt%).

The reducibility of 5%Ni-x% La₂O₃-ZrO₂ and 5%Ni-x% La₂O₃-Al₂O₃ (x = 0, 10, 15, and 20) catalysts were examined by TPR and the patterns are shown in Figure 2. For the 5%Ni-x% La₂O₃-ZrO₂ catalysts (Figure 2A), two prominent reduction maxima are detected over the entire temperature range, which may be attributed to the reduction of different NiO species (NiO→Ni⁰). The first reduction peak situated in region I at T_{max} = 298 °C could be ascribed to the reduction of free NiO that is not attached to the support, and hence reduces easily at low temperature. Further, the peak in the region II at T_{max} = 468 °C is allotted to the NiO reduction, attached to ZrO₂ by a moderately strong link and its reduction requires higher thermal energy. After support modification by means of La₂O₃, substantial variations in reduction kinetics were detected. Reduction maxima illustrating NiO reduction for the higher temperature peaks has shifted towards lower temperatures [42]. In the case of Figure 2B, the 5% Ni-x% La₂O₃-Al₂O₃ catalysts (x = 0, 10, 15, and 20) display a single peak in region III at higher temperatures. The un-promoted 5%Ni-Al₂O₃ catalyst shows a broad peak at 750 °C indicating that the reduced NiO is strongly attached to the support. When the support is modified with the addition of different loadings of La₂O₃, peaks of relatively lower areas appear at high temperatures. The La₂O₃ modified support catalyst is shifted to higher temperatures [43]. The highest La₂O₃ loading catalyst gives the highest peak shift. This means that the addition of La₂O₃ increases further the interaction between the NiO and the modified support. The

quantitative analysis of H₂ consumption during H₂-TPR is displayed in Table S2 of the supplementary.

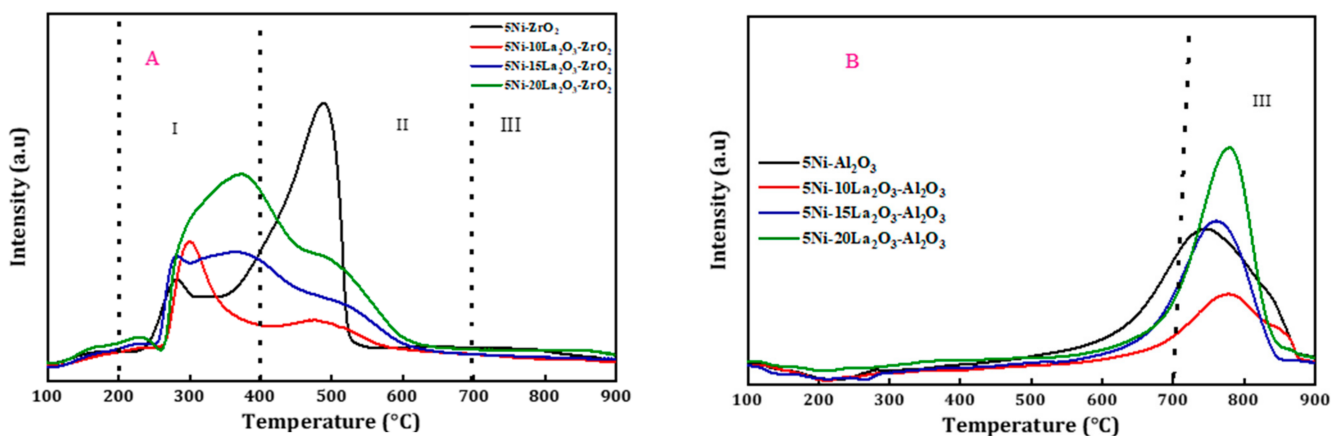


Figure 2. H₂-TPR profiles of (A) for 5Ni-xLa₂O₃-ZrO₂ and (B) 5Ni-xLa₂O₃-Al₂O₃ (x = 0, 10, 15, and 20 wt%) catalysts.

Figure 3 presents the powder X-ray diffraction patterns of the calcined 5Ni-xLa₂O₃-ZrO₂ and 5Ni-xLa₂O₃-Al₂O₃ catalysts (x = 0, 10, 15, and 20 wt%). Figure 3A displays the XRD patterns for 5Ni-xLa₂O₃-ZrO₂. There are no peaks attributable to La₂O₃ in these patterns since similar patterns are obtained for La₂O₃ modified and un-modified catalysts denoting the homogenous distribution of La₂O₃. The peaks at 28.3° and 31.6° are attributed to NiO phase (JCPDS No. 47–1049). The ZrO₂ support in Figure 3A has two crystalline phases, tetragonal zirconia (t-ZrO₂) and monoclinic zirconia (m-ZrO₂). The peaks at 25.5° and 34.3° are ascribed to m-ZrO₂ [44,45], while the peaks at 40.9°, 50.2°, and 55.5° are credited to t-ZrO₂ [46]. In Figure 3B, there is no peak ascribable to La₂O₃ in the patterns and therefore La₂O₃ is well dispersed in the alumina matrix. The characteristics peaks at 37.3° (311), 45.6° (400), and 67.0° (440), all are correspondingly allocated to the Al₂O₃ structure (JCPDS 10–0425) [47,48].

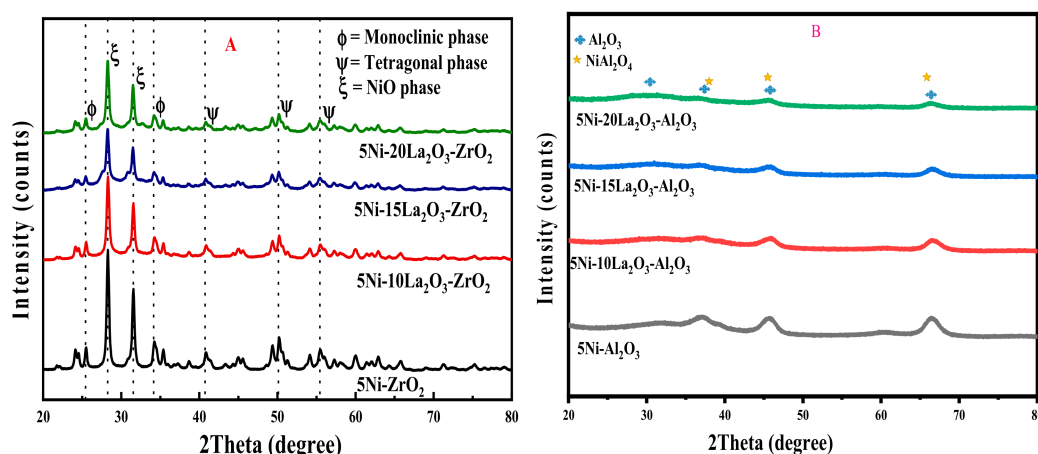


Figure 3. XRD patterns of the (A) 5Ni-xLa₂O₃+ZrO₂ (B) 5Ni-xLa₂O₃+Al₂O₃ catalysts (x = 0, 10, 15, and 20 wt%) calcined at 700 °C.

Figure 4 displays the hydrogen yield versus time on stream for the dry reforming reaction at 700 °C. The impact of La₂O₃ addition on the DRM catalytic performance of Ni-ZrO₂ is discussed in this section. The initial hydrogen yield of the 5Ni-ZrO₂ catalyst in Figure 4 is lower than the La₂O₃ modified catalysts. An evident trend is noted when La₂O₃ is added causing a significant improvement in the DRM performance. The improvement profile escalates as the following: 5Ni-ZrO₂ < 5Ni-20La₂O₃-ZrO₂ < 5Ni-15La₂O₃-ZrO₂ <

5Ni-10La₂O₃-ZrO₂. The highest hydrogen yield of about 80% is recorded using 10% La₂O₃. The improvement due to the La₂O₃ addition is attributed to the fact that La₂O₃ increases the dispersion of Ni particles on the supports and reduces the agglomeration of Ni particles during the reforming reaction as depicted in Figure 2A. Moreover, La₂O₃ increases the basicity as shown in the TPD profiles and therefore adsorb and react with CO₂ to form La₂O₂CO₃ species on the surface of catalyst which can speed up the conversion [49].

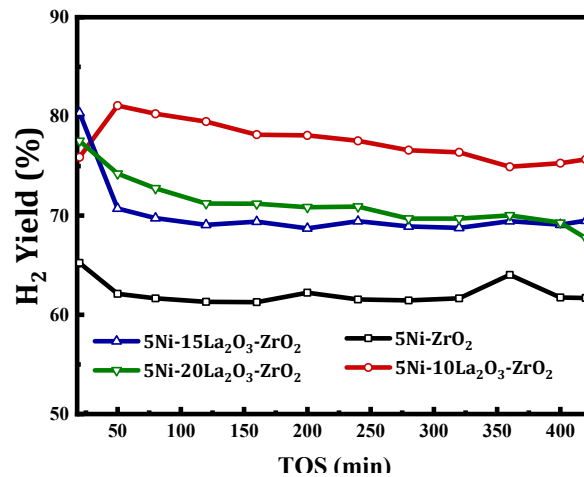


Figure 4. H₂ yield vs. time on stream over the 5Ni-xLa₂O₃-ZrO₂ (x = 0, 10, 15, and 20 wt%) catalysts at 700 °C for 420 min.

In Figure 5, the hydrogen yield obtained is close for La₂O₃ doped and non-doped catalysts. The La₂O₃ addition improved marginally the hydrogen yield in the following manner 5Ni-Al₂O₃ < 5Ni-20La₂O₃-Al₂O₃ < 5Ni-10La₂O₃-Al₂O₃ < 5Ni-15La₂O₃-Al₂O₃. The 15% La₂O₃ gave the highest hydrogen yield of 84%. It can be inferred that the effect of La₂O₃ loading affects differently the hydrogen yield productivity depending on the type of the support. Table 1 describes the efficiency of the present work and some of the literature.

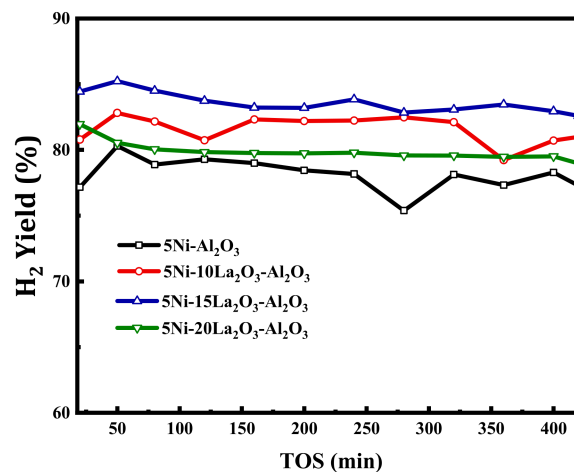


Figure 5. H₂ yield vs. time on stream over the 5Ni-xLa₂O₃-Al₂O₃ (x = 0, 10, 15, and 20 wt%) catalysts at 700 °C for 420 min.

Table 1. Hydrogen yield performances obtained in CO₂ reforming of methane of present and past work.

Catalyst	Feed (CH ₄ :CO ₂ :Inert)	Reaction Temperature (°C)	GHSV (mL/(g·h))	Yield (%)	Ref.
Ni/Zr-γAl ₂ O ₃	1:1:3	750	54,000	63	[50]
Ni@ZrO ₂ -SiZr-7.7	1:1:1	800	72,000	81	[51]
0.8% Ni+0.2% Co-MgAl ₂ O ₄	1:1:0.5	700	54,000	51	[52]
10Ni+1%Fe-MgAl ₂ O ₄	1:1:1	750	30,000	78	[53]
5Ni-10La ₂ O ₃ -ZrO ₂	1:1:0.33	700	42,000	80	This work
5Ni-15La ₂ O ₃ -Al ₂ O ₃	1:1:0.33	700	42,000	84	This work

Figure 6 exhibits the CO₂-TPD profiles of the (A) 5Ni-xLa₂O₃-ZrO₂ and (B) 5Ni-xLa₂O₃-Al₂O₃ (x = 0, 10, 15, and 20 wt%) spent catalysts obtained at 700 °C reaction temperature. This was performed to scan the surface basicity of the catalysts, which plays a vital role in the catalytic DRM reaction [54]. It is commonly understood that a greater desorption temperature of CO₂ reveals a stronger basicity and a bigger amount of CO₂ desorption although signifying that more basic sites are presented on the surface of catalyst [55]. In Figure 6A, three chief CO₂ desorption peaks were identified in the experimented temperature range from 50 to 700 °C for higher loadings of La₂O₃ (5Ni-15La₂O₃-ZrO₂ and 5Ni-20La₂O₃-ZrO₂) modified catalysts and only two peaks for the un-modified (5Ni-ZrO₂) and lower loading La₂O₃ (5Ni-10La₂O₃-ZrO₂) modified catalysts, which denoted that three types of basic sites existed in the 5Ni-xLa₂O₃ + ZrO₂ (x = 0, 10, 15, and 20 wt%) catalysts. The CO₂ desorption peaks appeared at 80 °C, 260 °C and 550 °C. The peaks correspond to the weak adsorption of CO₂ on OH groups, moderate adsorption of CO₂ and strong CO₂ adsorption on the metal–oxygen pairs and O²⁻ anions, respectively [56,57]. It is clear that CO₂ was favorably absorbed on the strong basic sites as the support was modified with La₂O₃, rather than bare zirconia support. This result showed that the adsorption of CO₂ had altered from physical adsorption to chemical adsorption because of the addition of La₂O₃. Figure 6B shows two main CO₂ desorption peaks at 80 °C and 250 °C corresponding to weak and moderate basic sites. Hence, the addition of La₂O₃ to the support did give significant variation in basicity of the 5Ni-xLa₂O₃ + Al₂O₃ catalysts. The 5Ni-15La₂O₃-Al₂O₃ displays larger peak intensity than the remaining catalysts, which is in accordance with the better activity observed. Table 2 shows a summary of a quantitative assessment of CO₂ adsorption of the spent catalysts via CO₂-TPD for ZrO₂ and Al₂O₃ supported catalysts.

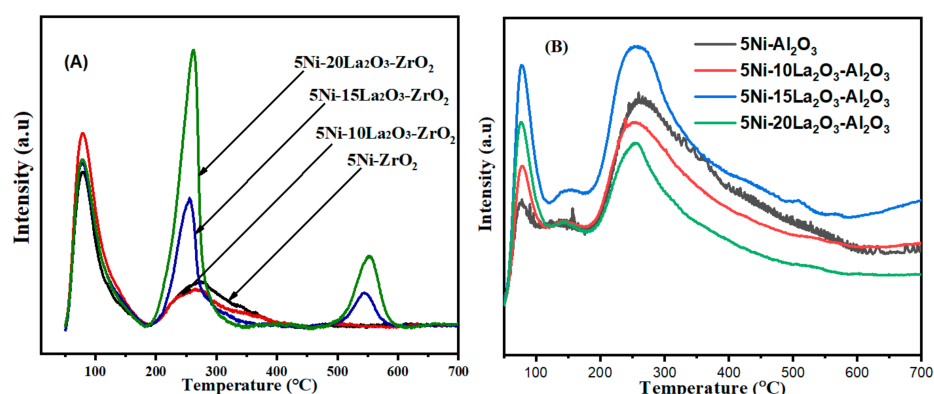
**Figure 6.** CO₂-TPD profiles of the spent (A) 5Ni-xLa₂O₃-ZrO₂ and (B) 5Ni-xLa₂O₃-Al₂O₃ (x = 0, 10, 15, and 20 wt%) catalysts obtained at 700 °C reaction temperature.

Table 2. Quantitative assessment of CO₂ adsorption of the spent catalysts via CO₂-TPD.

Catalyst	Weak-Basicity (μmol/g)	Medium-Basicity (μmol/g)	Strong-Basicity (μmol/g)	Total-Basicity (μmol/g)
5Ni-ZrO ₂ ^a	0.52	0.48	0.00	1
5Ni-10La ₂ O ₃ -ZrO ₂	0.66	0.29	0.00	0.95
5Ni-15La ₂ O ₃ -ZrO ₂	0.63	0.49	0.12	1.24
5Ni-20La ₂ O ₃ -ZrO ₂	0.52	0.94	0.27	1.73
5Ni-Al ₂ O ₃ ^a	0.44	0.38	0.18	1
5Ni-10La ₂ O ₃ -Al ₂ O ₃	0.42	0.11	0.00	0.53
5Ni-15La ₂ O ₃ -Al ₂ O ₃	0.32	0.10	0.00	0.42
5Ni-20La ₂ O ₃ -Al ₂ O ₃	0.35	0.06	0.00	0.41

^a For comparison and basicity assessment of catalysts, the sum of all basic sites of 5Ni-ZrO₂ is set to 1 and 5Ni-Al₂O₃ is set to 1.

Figure 7A,B contain images obtained from Energy-dispersive X-ray spectroscopy (EDX) analysis of the fresh samples of both 5Ni-10La₂O₃-ZrO₂ and 5Ni-15La₂O₃-Al₂O₃. These results show the elemental composition of the as-prepared catalyst samples. First, the analysis confirmed the presence of all the elemental constituents that were mixed together during the catalyst synthesis. Moreover, the percentage loadings revealed by the EDX analysis are virtually the same as intended in the calculation and catalyst preparation with error values of 10% for Ni and 6% for La.

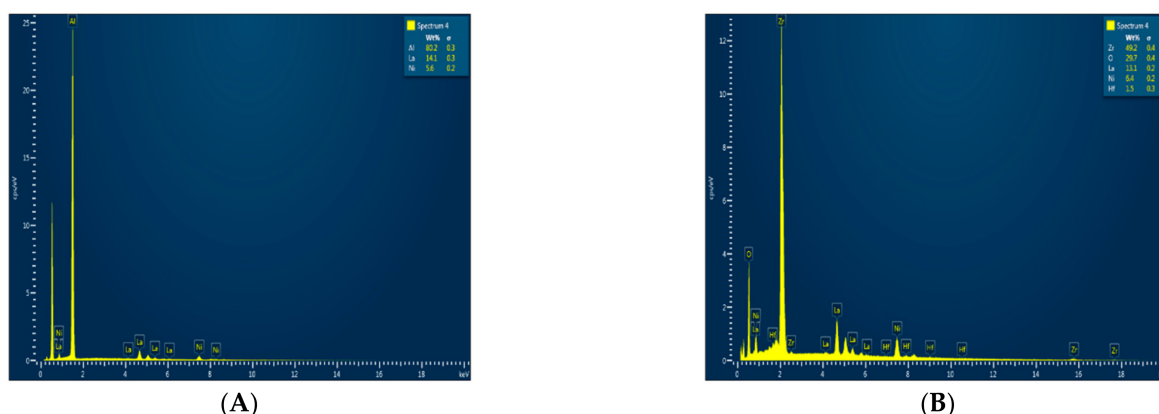


Figure 7. EDX analysis of fresh (A) 5Ni-15La₂O₃-Al₂O₃ and (B) 5Ni-10La₂O₃-ZrO₂ showing the elemental composition of prepared catalysts.

Broad examination of the morphology of catalysts was performed via TEM. Typical TEM overviews of the fresh catalysts (Figure 8A,C) and spent catalyst samples (Figure 8B,D) were acquired after DRM at 700 °C for 420 min time on stream. There is a difference in the morphology of the fresh and used catalysts. The fresh catalyst seems to have particles clumped on the surface, while the spent catalysts depict rough and dispersed particles on the catalyst surface. In addition to the recognized metal particles, carbon in the form of nanotubes can be seen in the images of the used catalysts. The image of the fresh 5Ni-10La₂O₃-ZrO₂ catalyst is shown in Figure 8A. It is evident from the TEM images that the Ni is homogeneously dispersed over the surface of the support. In contrast to its spent sample as shown in Figure 8B, big quantities of coke are formed commonly in the form of nanotubes. The TEM images showed well dispersed Ni species ((average particle diameter of 4 nm) over La₂O₃-Al₂O₃ support (Figure 8C). However, after the reaction (Figure 8D) size of Ni species has grown (average particle diameter of 7–8 nm).

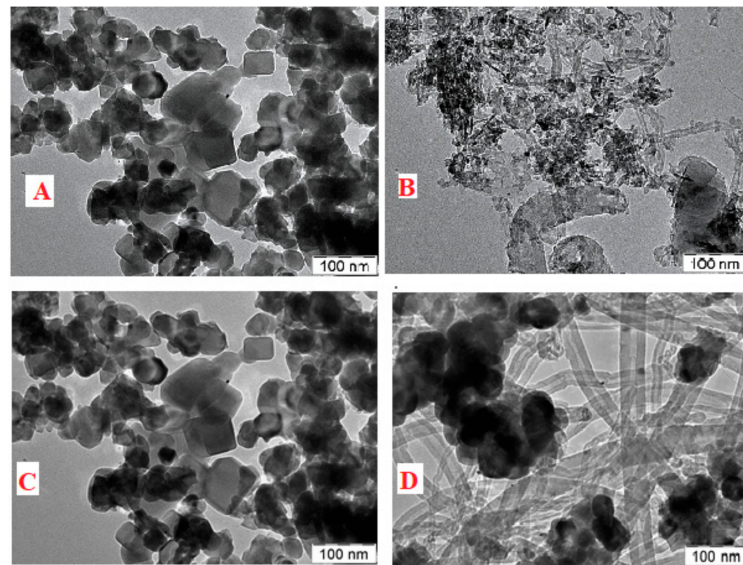


Figure 8. TEM image of (A) Fresh, (B) spent of 5Ni/10La₂O₃+ZrO₂, (C) Fresh, (D) spent of 5Ni/15La₂O₃ + Al₂O₃ catalysts.

The Fourier Transform Infrared Spectroscopy (FTIR) analysis of fresh 5Ni-ZrO₂, 5Ni-10La₂O₃-ZrO₂, 5Ni-Al₂O₃ and 5Ni-15La₂O₃-Al₂O₃ catalysts were done to investigate the existing bonds within the catalyst system. The infrared spectra of absorption for these samples are shown in Figure 9A,B.

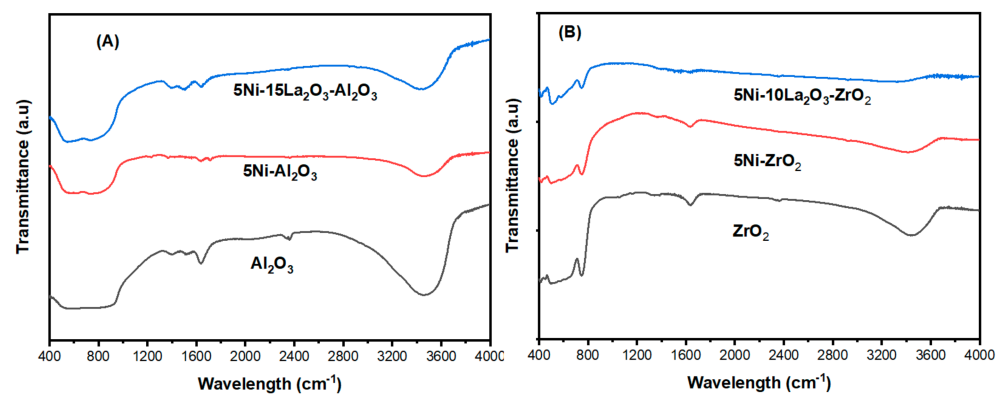


Figure 9. The FTIR spectra of fresh (A) Al₂O₃, 5Ni-Al₂O₃, 5Ni-15La₂O₃-Al₂O₃ and (B) ZrO₂, 5Ni-ZrO₂, 5Ni-10La₂O₃-ZrO₂ showing the existing stretching vibration.

In Figure 9A, Al₂O₃ is well known for its tendency to adsorb moisture from the atmosphere onto itself. Thus, the distinct band representing the stretching vibration of O-H, within the wavelengths 3430–3460 cm⁻¹ for all the samples can be ascribed to [OH]⁻¹ groups interaction and/or physisorbed moisture interaction that is adsorbed onto the Al₂O₃ support [58]. It is noticeable from the figure that the extent of hydration of the catalyst surface changed with metal addition as the OH band's intensity decreased on adding active metal. Moreover, the vibration bands centered at around 1400, 1520, 1649, and 2366 cm⁻¹ can be seen for the support and the other samples. This implies that these bands can be associated with the support, the Al–O bond stretching to be specific [59]. The small less noticeable peaks appearing at wavelengths 1237 and 1719 cm⁻¹ for the 5Ni-Al₂O₃ sample can be said to be the stretching vibration of NiO and NiAl₂O₄ species, respectively. The latter is thought to have stronger interaction with the support, in light of that it appeared at a higher wavelength.

As for the ZrO_2 support and ZrO_2 supported catalysts (Figure 9B); the band within $3357\text{--}3440\text{ cm}^{-1}$ can be said to be hydrogen-bonded bending and stretching of the OH groups as a result of adsorbed moisture while the peaks at $1632\text{--}1640\text{ cm}^{-1}$ can be assigned to the vibration of the water molecules [60]. These peaks are seen to decrease in intensity with the addition of nickel and lanthanum oxide to the support. The peaks that are centered at around 457 and 752 cm^{-1} represent the asymmetric stretching of the $\text{Zr}\text{--O}\text{--Zr}$ bond [61]. The vibration owing to the presence of La_2O_3 was not discovered. This further supports the results obtained from the XRD analysis of samples with La_2O_3 .

Figure 10A displays TGA profiles of spent $5\text{Ni}\text{--}x\text{La}_2\text{O}_3\text{--ZrO}_2$ ($x = 0, 10, 15,$ and $20\text{ wt}\%$) catalysts operated at $700\text{ }^\circ\text{C}$. The weight loss above $500\text{ }^\circ\text{C}$ was due to the removal of deposited carbon. The extents of carbon deposition on the spent catalysts exhibit the following sequence: $5\text{Ni}\text{--}10\text{La}_2\text{O}_3\text{--ZrO}_2 < 5\text{Ni}\text{--}15\text{La}_2\text{O}_3\text{--ZrO}_2 < 5\text{Ni}\text{--}20\text{La}_2\text{O}_3\text{--ZrO}_2 < 5\text{Ni}\text{--ZrO}_2$. The un-promoted ZrO_2 catalyst gives the highest weight loss of 47.4% . The results are well established with the catalytic performance. Similarly, Figure 9B shows the TGA profiles of spent $5\text{Ni}\text{--}x\text{La}_2\text{O}_3\text{--Al}_2\text{O}_3$ ($x = 0, 10, 15,$ and $20\text{ wt}\%$) catalysts at $700\text{ }^\circ\text{C}$. The amounts of weight loss are close to each between the La_2O_3 promoted and non-promoted catalysts. Since values range between 9.0% for $5\text{Ni}\text{--}10\text{La}_2\text{O}_3\text{--Al}_2\text{O}_3$ and 17.2% for $5\text{Ni}\text{--ZrO}_2$, this indicates the Al_2O_3 supported catalysts are more resistant to carbon deposition than ZrO_2 supported catalysts.

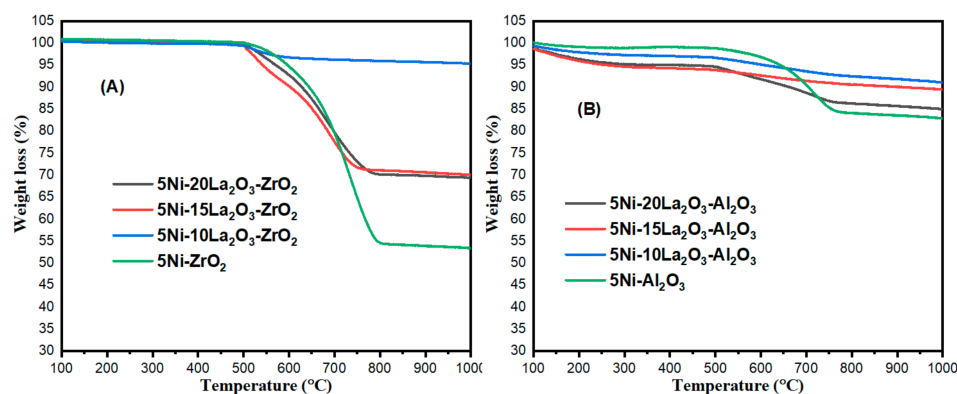


Figure 10. TGA profiles of spent (A) $5\text{Ni}\text{--}x\text{La}_2\text{O}_3\text{--ZrO}_2$, (B) $5\text{Ni}\text{--}x\text{La}_2\text{O}_3\text{--Al}_2\text{O}_3$ ($x = 0, 10, 15,$ and $20\text{ wt}\%$) catalysts at $700\text{ }^\circ\text{C}$.

Figure 11 shows the Raman analysis of the used catalysts ($5\text{Ni}\text{--ZrO}_2$, $5\text{Ni}\text{--}10\text{La}_2\text{O}_3\text{--ZrO}_2$, $5\text{Ni}\text{--Al}_2\text{O}_3$, and $5\text{Ni}\text{--}15\text{La}_2\text{O}_3\text{--Al}_2\text{O}_3$). The D (deformation) and G (graphitic) bands appear at nearly 1342 and 1580 cm^{-1} respectively except for spent $5\text{Ni}\text{--Al}_2\text{O}_3$ with D and G bands appearing at about 1468 and 1532 cm^{-1} , respectively. The spent catalysts are characterized by carbon deposits of different degree of graphitization. It is established that carbon deposits having high I_G to I_D ratio show better extent of graphitization [62]. From the figure, it can be seen that $5\text{Ni}\text{--ZrO}_2$ had the highest degree of graphitization followed by $5\text{Ni}\text{--Al}_2\text{O}_3$. Moreover, it can be inferred that the graphitization decreases with the addition of La_2O_3 . Thus, La_2O_3 promotes the formation carbons that are defective.

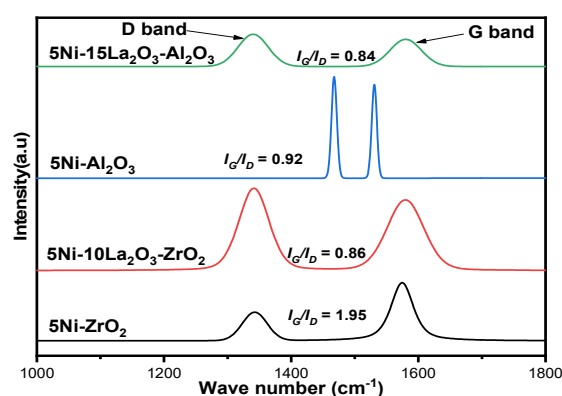


Figure 11. Raman spectra for the spent catalysts (5Ni-ZrO₂, 5Ni-10La₂O₃-ZrO₂, 5Ni-Al₂O₃, and 5Ni-15La₂O₃-Al₂O₃) showing the extent of graphitization of the carbon deposits.

4. Conclusions

This paper elucidates the role of La₂O₃ addition to two different supports (ZrO₂ and Al₂O₃) of Ni-based catalysts for the hydrogen production via CO₂ reforming of methane. The 5Ni-10La₂O₃-ZrO₂ catalyst increased the hydrogen yield by 25% in comparison with the pristine 5Ni-ZrO₂. Similarly, the 5Ni-15La₂O₃-Al₂O₃ catalyst showed improved efficiency of 8% of hydrogen yield. The La₂O₃ loading influenced differently the ZrO₂ and the Al₂O₃ supports. The study displayed that the modified La₂O₃-Al₂O₃ support catalysts gave a higher hydrogen yield than La₂O₃-ZrO₂ supported catalyst. The catalyst characterizations showed that La₂O₃ addition improved specific surface areas, dispersion, reducibility, metal–support interaction, and surface basic sites which contributed towards the enhanced hydrogen yield. The qualitative and quantitative analysis of carbon formed over the spent catalysts using TEM, TGA, and Raman spectroscopy showed presence of carbon nanotubes. This work provides an insight towards the role of support modification during DRM.

Supplementary Materials: The following are available online at <https://www.mdpi.com/article/10.3390/en14092412/s1>, Table S1: Textural properties of different catalysts supported Ni catalysts: BET specific surface area (S_{BET}), pore volume (P_V), and pore diameter (D_P), Table S2: The quantitative analysis of H₂ consumption during H₂-TPR.

Author Contributions: A.A.-F., A.I. and S.K. synthesized the catalysts, carried out all the experiments and characterization tests, and wrote the manuscript. W.K. and M.S. prepared the catalyst and contributed to proofreading of the manuscript. A.A. and A.F. contributed to the analysis of the data and writing—review of the manuscript. All authors have read and agreed to the published version of the manuscript.

Funding: This research was funded by Deanship of Scientific Research at King Saud University so the authors would like to express their sincere appreciation to the Deanship of Scientific Research at King Saud University for funding this research project (#RG-119).

Institutional Review Board Statement: Not applicable.

Informed Consent Statement: Not applicable.

Data Availability Statement: Not applicable.

Acknowledgments: The authors would like to express their sincere appreciation to the Deanship of Scientific Research at King Saud University for funding this research project (#RG-119).

Conflicts of Interest: The authors declare no conflict of interest.

References

1. Wang, Q.; Chen, X.; Jha, A.N.; Rogers, H. Natural gas from shale formation—The evolution, evidences and challenges of shale gas revolution in United States. *Renew. Sustain. Energy Rev.* **2014**, *30*, 1–28. [[CrossRef](#)]

2. Montgomery, C.T.; Smith, M.B. Hydraulic Fracturing: History of an Enduring Technology. *J. Pet. Technol.* **2010**, *62*, 26–40. [[CrossRef](#)]
3. Themelis, N.J.; Ulloa, P.A. Methane generation in landfills. *Renew. Energy* **2007**, *32*, 1243–1257. [[CrossRef](#)]
4. Izquierdo, U.; Barrio, V.; Requies, J.; Cambra, J.; Güemez, M.; Arias, P. Tri-reforming: A new biogas process for synthesis gas and hydrogen production. *Int. J. Hydrog. Energy* **2013**, *38*, 7623–7631. [[CrossRef](#)]
5. Al-Fatesh, A.S.; Kumar, R.; Kasim, S.O.; Ibrahim, A.A.; Fakeeha, A.H.; Abasaeed, A.E.; Alrasheed, R.; Bagabas, A.; Chaudhary, M.L.; Frusteri, F.; et al. The effect of modifier identity on the performance of Ni-based catalyst supported on γ -Al₂O₃ in dry reforming of methane. *Catal. Today* **2020**, *348*, 236–242. [[CrossRef](#)]
6. Ibrahim, A.A.; Al-Fatesh, A.S.; Khan, W.U.; Kasim, S.O.; Abasaeed, A.E.; Fakeeha, A.H.; Bonura, G.; Frusteri, F. Enhanced coke suppression by using phosphate-zirconia supported nickel catalysts under dry methane reforming conditions. *Int. J. Hydrog. Energy* **2019**, *44*, 27784–27794. [[CrossRef](#)]
7. Al-Fatesh, A.S.; Abu-Dahrieh, J.K.; Atia, H.; Armbruster, U.; Ibrahim, A.A.; Khan, W.U.; Abasaeed, A.E.; Fakeeha, A.H. Effect of pre-treatment and calcination temperature on Al₂O₃-ZrO₂ supported Ni-Co catalysts for dry reforming of methane. *Int. J. Hydrog. Energy* **2019**, *44*, 21546–21558. [[CrossRef](#)]
8. Zhang, S.; Muratsugu, S.; Ishiguro, N.; Tada, M. Ceria-Doped Ni/SBA-16 Catalysts for Dry Reforming of Methane. *ACS Catal.* **2013**, *3*, 1855–1864. [[CrossRef](#)]
9. Boyano, A.; Morosuk, T.; Blanco-Marigorta, A.; Tsatsaronis, G. Conventional and advanced exergoenvironmental analysis of a steam methane reforming reactor for hydrogen production. *J. Clean. Prod.* **2012**, *20*, 152–160. [[CrossRef](#)]
10. Kim, A.R.; Lee, H.Y.; Cho, J.M.; Choi, J.-H.; Bae, J.W. Ni/M-Al₂O₃ (M=Sm, Ce or Mg) for combined steam and CO₂ reforming of CH₄ from coke oven gas. *J. CO₂ Util.* **2017**, *21*, 211–218. [[CrossRef](#)]
11. Lougou, B.G.; Shuai, Y.; Chaffa, G.; Xing, H.; Tan, H.; Du, H. Analysis of CO₂ utilization into synthesis gas based on solar thermochemical CH₄-reforming. *J. Energy Chem.* **2019**, *28*, 61–72. [[CrossRef](#)]
12. Wu, Z.; Yang, B.; Miao, S.; Liu, W.; Xie, J.; Lee, S.; Pellin, M.J.; Xiao, D.; Su, D.; Ma, D. Lattice Strained Ni-Co alloy as a High-Performance Catalyst for Catalytic Dry Reforming of Methane. *ACS Catal.* **2019**, *9*, 2693–2700. [[CrossRef](#)]
13. Arora, S.; Prasad, R. An overview on dry reforming of methane: Strategies to reduce carbonaceous deactivation of catalysts. *RSC Adv.* **2016**, *6*, 108668–108688. [[CrossRef](#)]
14. Varga, E.; Pusztai, P.; Steinrück, H.-P.; Óvári, L.; Papp, C.; Kónya, Z.; Oszkó, A.; Erdőhelyi, A.; Kiss, J. Probing the interaction of Rh, Co and bimetallic Rh–Co nanoparticles with the CeO₂ support: Catalytic materials for alternative energy generation. *Phys. Chem. Chem. Phys.* **2015**, *17*, 27154–27166. [[CrossRef](#)]
15. Pakhare, D.; Spivey, J. A review of dry (CO₂) reforming of methane over noble metal catalysts. *Chem. Soc. Rev.* **2014**, *43*, 7813–7837. [[CrossRef](#)] [[PubMed](#)]
16. Damyanova, S.; Shtereva, I.; Pawelec, B.; Mihaylov, L.; Fierro, J.L.G. Characterization of none and yttrium-modified Ni-based catalysts for dry reforming of methane. *Appl. Catal. B Environ.* **2020**, *278*, 119335. [[CrossRef](#)]
17. Jalali, R.; Rezaei, M.; Nematollahi, B.; Baghalha, M. Preparation of Ni/MeAl₂O₄-MgAl₂O₄ (Me=Fe, Co, Ni, Cu, Zn, Mg) nanocatalysts for the syngas production via combined dry reforming and partial oxidation of methane. *Renew. Energy* **2020**, *149*, 1053–1067. [[CrossRef](#)]
18. Liu, C.-J.; Ye, J.; Jiang, J.; Pan, Y. Progresses in the Preparation of Coke Resistant Ni-based Catalyst for Steam and CO₂ Reforming of Methane. *ChemCatChem* **2011**, *3*, 529–541. [[CrossRef](#)]
19. Wang, N.; Shen, K.; Yu, X.; Qian, W.; Chu, W. Preparation and characterization of a plasma treated NiMgSBA-15 catalyst for methane reforming with CO₂ to produce syngas. *Catal. Sci. Technol.* **2013**, *3*, 2278–2287. [[CrossRef](#)]
20. Bradford, M.C.; Vannice, M.A. The role of metal–support interactions in CO₂ reforming of CH₄. *Catal. Today* **1999**, *50*, 87–96. [[CrossRef](#)]
21. Tang, M.; Liu, K.; Roddick, D.M.; Fan, M. Enhanced lattice oxygen reactivity over Fe₂O₃/Al₂O₃ redox catalyst for chemical-looping dry (CO₂) reforming of CH₄: Synergistic La-Ce effect. *J. Catal.* **2018**, *368*, 38–52. [[CrossRef](#)]
22. Faria, E.; Neto, R.; Colman, R.; Noronha, F. Hydrogen production through CO₂ reforming of methane over Ni/CeZrO₂/Al₂O₃ catalysts. *Catal. Today* **2014**, *228*, 138–144. [[CrossRef](#)]
23. Stagg-Williams, S.M.; Noronha, F.B.; Fendley, G.; Resasco, D.E. CO₂ Reforming of CH₄ over Pt/ZrO₂ Catalysts Promoted with La and Ce Oxides. *J. Catal.* **2000**, *194*, 240–249. [[CrossRef](#)]
24. Li, Z.-X.; Shi, F.-B.; Li, L.-L.; Zhang, T.; Yan, C.-H. A facile route to ordered mesoporous-alumina-supported catalysts, and their catalytic activities for CO oxidation. *Phys. Chem. Chem. Phys.* **2010**, *13*, 2488–2491. [[CrossRef](#)] [[PubMed](#)]
25. Dehimi, L.; Benguerba, Y.; Virginie, M.; Hijazi, H. Microkinetic modelling of methane dry reforming over Ni/Al₂O₃ catalyst. *Int. J. Hydrog. Energy* **2017**, *42*, 18930–18940. [[CrossRef](#)]
26. Lašič Jurković, D.; Liu, J.-L.; Pohar, A.; Likozar, B. Methane Dry Reforming over Ni/Al₂O₃ Catalyst in Spark Plasma Reactor: Linking Computational Fluid Dynamics (CFD) with Reaction Kinetic Modelling. *Catal. Today* **2021**, *362*, 11–21. [[CrossRef](#)]
27. Bian, Z.; Zhong, W.; Yu, Y.; Wang, Z.; Jiang, B.; Kawi, S. Dry reforming of methane on Ni/mesoporous-Al₂O₃ catalysts: Effect of calcination temperature. *Int. J. Hydrog. Energy* **2021**. [[CrossRef](#)]
28. Newnham, J.; Mantri, K.; Amin, M.H.; Tardio, J.; Bhargava, S.K. Highly stable and active Ni-mesoporous alumina catalysts for dry reforming of methane. *Int. J. Hydrog. Energy* **2012**, *37*, 1454–1464. [[CrossRef](#)]

29. Montoya, J.; Romero-Pascual, E.; Gimón, C.; Del Angel, P.; Monzón, A. Methane reforming with CO₂ over Ni/ZrO₂-CeO₂ catalysts prepared by sol-gel. *Catal. Today* **2000**, *63*, 71–85. [[CrossRef](#)]
30. Li, W.; Zhao, Z.; Jiao, Y. Dry reforming of methane towards CO-rich hydrogen production over robust supported Ni catalyst on hierarchically structured monoclinic zirconia nanosheets. *Int. J. Hydrog. Energy* **2016**, *41*, 17907–17921. [[CrossRef](#)]
31. Jang, J.T.; Yoon, K.J.; Bae, J.W.; Han, G.Y. Cyclic production of syngas and hydrogen through methane-reforming and water-splitting by using ceria-zirconia solid solutions in a solar volumetric receiver-reactor. *Sol. Energy* **2014**, *109*, 70–81. [[CrossRef](#)]
32. Hu, X.; Jia, X.; Zhang, X.; Liu, Y.; Liu, C.-J. Improvement in the activity of Ni/ZrO₂ by cold plasma decomposition for dry reforming of methane. *Catal. Commun.* **2019**, *128*, 105720. [[CrossRef](#)]
33. Zhang, M.; Zhang, J.; Zhou, Z.; Chen, S.; Zhang, T.; Song, F.; Zhang, Q.; Tsubaki, N.; Tan, Y.; Han, Y. Effects of the surface adsorbed oxygen species tuned by rare-earth metal doping on dry reforming of methane over Ni/ZrO₂ catalyst. *Appl. Catal. B Environ.* **2020**, *264*, 118522. [[CrossRef](#)]
34. Zhang, W.; Liu, B.; Zhu, C.; Tian, Y. Preparation of La₂NiO₄/ZSM-5 catalyst and catalytic performance in CO₂/CH₄ reforming to syngas. *Appl. Catal. A Gen.* **2005**, *292*, 138–143. [[CrossRef](#)]
35. Horváth, A.; Stefler, G.; Geszti, O.; Kienneman, A.; Pietraszek, A.; Guzzi, L. Methane dry reforming with CO₂ on CeZr-oxide supported Ni, NiRh and NiCo catalysts prepared by sol-gel technique: Relationship between activity and coke formation. *Catal. Today* **2011**, *169*, 102–111. [[CrossRef](#)]
36. Tran, N.T.; Van Le, Q.; Van Cuong, N.; Nguyen, T.D.; Phuc, N.H.H.; Phuong, P.T.; Monir, M.U.; Aziz, A.A.; Truong, Q.D.; Abidin, S.Z.; et al. La-doped cobalt supported on mesoporous alumina catalysts for improved methane dry reforming and coke mitigation. *J. Energy Inst.* **2020**, *93*, 1571–1580. [[CrossRef](#)]
37. Liu, H.; Hadjiltaief, H.B.; Benzina, M.; Gálvez, M.E.; Da Costa, P. Natural clay based nickel catalysts for dry reforming of methane: On the effect of support promotion (La, Al, Mn). *Int. J. Hydrog. Energy* **2019**, *44*, 246–255. [[CrossRef](#)]
38. Yabe, T.; Mitarai, K.; Oshima, K.; Ogo, S.; Sekine, Y. Low-temperature dry reforming of methane to produce syngas in an electric field over La-doped Ni/ZrO₂ catalysts. *Fuel Process. Technol.* **2017**, *158*, 96–103. [[CrossRef](#)]
39. Al-Fatesh, A.S.; Arafat, Y.; Ibrahim, A.A.; Kasim, S.O.; Alharthi, A.; Fakeeha, A.H.; Abasaheed, A.E.; Bonura, G.; Frusteri, F. Catalytic Behaviour of Ce-Doped Ni Systems Supported on Stabilized Zirconia under Dry Reforming Conditions. *Catalysts* **2019**, *9*, 473. [[CrossRef](#)]
40. Mandal, S.; Santra, C.; Kumar, R.; Pramanik, M.; Rahman, S.; Bhaumik, A.; Maity, S.; Sen, D.; Chowdhury, B. Niobium doped hexagonal mesoporous silica (HMS-X) catalyst for vapor phase Beckmann rearrangement reaction. *RSC Adv.* **2014**, *4*, 845–854. [[CrossRef](#)]
41. Rahman, S.; Santra, C.; Kumar, R.; Bahadur, J.; Sultana, A.; Schweins, R.; Sen, D.; Maity, S.; Mazumdar, S.; Chowdhury, B. Highly active Ga promoted Co-HMS-X catalyst towards styrene epoxidation reaction using molecular O₂. *Appl. Catal. A Gen.* **2014**, *482*, 61–68. [[CrossRef](#)]
42. Jiang, X.-Y.; Zhou, R.-X.; Pan, P.; Zhu, B.; Yuan, X.-X.; Zheng, X.-M. Effect of the addition of La₂O₃ on TPR and TPD of CuO_γ-Al₂O₃ catalysts. *Appl. Catal. A Gen.* **1997**, *150*, 131–141. [[CrossRef](#)]
43. Mo, W.; Ma, F.; Ma, Y.; Fan, X. The optimization of Ni-Al₂O₃ catalyst with the addition of La₂O₃ for CO₂-CH₄ reforming to produce syngas. *Int. J. Hydrog. Energy* **2019**, *44*, 24510–24524. [[CrossRef](#)]
44. Goula, M.; Charisiou, N.; Siakavelas, G.; Tzounis, L.; Tsiaoussis, I.; Panagiotopoulou, P.; Goula, G.; Yentekakis, I. Syngas production via the biogas dry reforming reaction over Ni supported on zirconia modified with CeO₂ or La₂O₃ catalysts. *Int. J. Hydrog. Energy* **2017**, *42*, 13724–13740. [[CrossRef](#)]
45. Zhang, J.; Gao, Y.; Jia, X.; Wang, J.; Chen, Z.; Xu, Y. Oxygen vacancy-rich mesoporous ZrO₂ with remarkably enhanced visible-light photocatalytic performance. *Sol. Energy Mater. Sol. Cells* **2018**, *182*, 113–120. [[CrossRef](#)]
46. Titus, J.; Roussière, T.; Wasserschaff, G.; Schunk, S.; Milanov, A.; Schwab, E.; Wagner, G.; Oeckler, O.; Gläser, R. Dry reforming of methane with carbon dioxide over NiO-MgO-ZrO₂. *Catal. Today* **2016**, *270*, 68–75. [[CrossRef](#)]
47. Alipour, Z.; Rezaei, M.; Meshkani, F. Effects of support modifiers on the catalytic performance of Ni/Al₂O₃ catalyst in CO₂ reforming of methane. *Fuel* **2014**, *129*, 197–203. [[CrossRef](#)]
48. Mierczynski, P.; Mierczynska, A.; Ciesielski, R.; Mosinska, M.; Nowosielska, M.; Czyrkowska, A.; Maniukiewicz, W.; Szyrkowska, M.I.; Vasilev, K. High Active and Selective Ni/CeO₂-Al₂O₃ and Pd-Ni/CeO₂-Al₂O₃ Catalysts for Oxy-Steam Reforming of Methanol. *Catalysts* **2018**, *8*, 380. [[CrossRef](#)]
49. Li, K.; Pei, C.; Li, X.; Chen, S.; Zhang, X.; Liu, R.; Gong, J. Dry reforming of methane over La₂O₂CO₃-modified Ni/Al₂O₃ catalysts with moderate metal support interaction. *Appl. Catal. B Environ.* **2020**, *264*, 118448. [[CrossRef](#)]
50. Khani, Y.; Bahadoran, F.; Shariatnia, Z.; Varmazyari, M.; Safari, N. Synthesis of highly efficient and stable Ni/CexZr1-xGdxO₄ and Ni/X-Al₂O₃ (X = Ce, Zr, Gd, Ce-Zr-Gd) nanocatalysts applied in methane reforming reactions. *Ceram. Int.* **2020**, *46*, 25122–25135. [[CrossRef](#)]
51. Lim, Z.-Y.; Tu, J.; Xu, Y.; Chen, B. Ni@ZrO₂ yolk-shell catalyst for CO₂ methane reforming: Effect of Ni@SiO₂ size as the hard-template. *J. Colloid Interface Sci.* **2021**, *590*, 641–651. [[CrossRef](#)]
52. Aghaali, M.H.; Firoozi, S. Enhancing the catalytic performance of Co substituted NiAl₂O₄ spinel by ultrasonic spray pyrolysis method for steam and dry reforming of methane. *Int. J. Hydrog. Energy* **2021**, *46*, 357–373. [[CrossRef](#)]

53. Medeiros, R.L.; Macedo, H.P.; Melo, V.R.; Oliveira, Â.A.S.; Barros, J.M.; Melo, M.A.; Melo, D.M. Ni supported on Fe-doped MgAl_2O_4 for dry reforming of methane: Use of factorial design to optimize H_2 yield. *Int. J. Hydrog. Energy* **2016**, *41*, 14047–14057. [[CrossRef](#)]
54. Lavoie, J.-M. Review on dry reforming of methane, a potentially more environmentally-friendly approach to the increasing natural gas exploitation. *Front. Chem.* **2014**, *2*, 81. [[CrossRef](#)]
55. Zhang, L.; Zhang, Q.; Liu, Y.; Zhang, Y. Dry reforming of methane over Ni/MgO- Al_2O_3 catalysts prepared by two-step hydrothermal method. *Appl. Surf. Sci.* **2016**, *389*, 25–33. [[CrossRef](#)]
56. Wang, H.; Zhao, B.; Qin, L.; Wang, Y.; Yu, F.; Han, J. Non-thermal plasma-enhanced dry reforming of methane and CO_2 over Ce-promoted Ni/C catalysts. *Mol. Catal.* **2020**, *485*, 110821. [[CrossRef](#)]
57. Zheng, X.; Li, Y.; Zhang, L.; Shen, L.; Xiao, Y.; Zhang, Y.; Au, C.; Jiang, L. Insight into the effect of morphology on catalytic performance of porous CeO_2 nanocrystals for H_2S selective oxidation. *Appl. Catal. B Environ.* **2019**, *252*, 98–110. [[CrossRef](#)]
58. Lei, H.; Zhang, P. Preparation of alumina/silica core-shell abrasives and their CMP behavior. *Appl. Surf. Sci.* **2007**, *253*, 8754–8761. [[CrossRef](#)]
59. Sanchez, E.A.; Comelli, R.A. Hydrogen by glycerol steam reforming on a nickel–alumina catalyst: Deactivation processes and regeneration. *Int. J. Hydrog. Energy* **2012**, *37*, 14740–14746. [[CrossRef](#)]
60. Goharshadi, E.K.; Hadadian, M. Effect of calcination temperature on structural, vibrational, optical, and rheological properties of zirconia nanoparticles. *Ceram. Int.* **2012**, *38*, 1771–1777. [[CrossRef](#)]
61. Heshmatpour, F.; Aghakhanpour, R.B. Synthesis and characterization of superfine pure tetragonal nanocrystalline sulfated zirconia powder by a non-alkoxide sol–gel route. *Adv. Powder Technol.* **2012**, *23*, 80–87. [[CrossRef](#)]
62. Kim, S.; Crandall, B.S.; Lance, M.J.; Cordonnier, N.; Lauterbach, J.; Sasmaz, E. Activity and stability of NiCe@SiO multi-yolk-shell nanotube catalyst for tri-reforming of methane. *Appl. Catal. B Environ.* **2019**, *259*, 118037. [[CrossRef](#)]